



Cite this: *RSC Adv.*, 2018, 8, 25008

Fabrication of a scratch & heat resistant superhydrophobic SiO₂ surface with self-cleaning and semi-transparent performance

Xiaolu Zhao,^a Ji Li,^a ^{*,a} Qiao Li,^a Liang Qiao,^b Lei Zhang,^a Zhu Liu^a and Chunhui Yang ^a

Herein, we report the fabrication of a superhydrophobic surface with a new and effective silica nanocomposite. A facile synthesis was developed by spraying the as-prepared silica suspension on a glass substrate, where the SiO₂ nanoparticles were composed of methylated aerogel particles wrapped by hydroxyl-terminated polydimethylsiloxane (PDMS). Three types of methylated silica aerogel nanoparticles with different surface roughness and porosities were prepared using specific precursors and methylation agents. The coating of the silica aerogels (sodium silicate and trimethylchlorosilane) wrapped in PDMS was exceptionally superhydrophobic with a superior water contact angle of 169.80 ± 3° and a sliding angle of less than 4°. The semi-transparent coating maintained its excellent water repellency at 350 °C for at least 4 h and exhibited durable superhydrophobic properties for 6 months at ambient conditions. Additionally, the coating also showed good mechanical stability and remarkable self-cleaning behaviour.

Received 23rd May 2018
Accepted 25th June 2018

DOI: 10.1039/c8ra04383c

rsc.li/rsc-advances

1. Introduction

Superhydrophobic surfaces, with a water contact angle greater than 150° and a sliding angle (the difference between the advancing and receding contact angles) of less than 10°,¹ have received increasing attention from both academic and practical fields such as self-cleaning,^{2,3} anti-corrosion,^{4,5} oil-water separation,^{6,7} and anti-icing.^{8,9} The prevalent fabrication approaches for superhydrophobic surfaces include etching,¹⁰ physical/chemical vapour deposition,^{11,12} electro-spinning,¹³ nano/microparticle assembly,^{14,15} the template method,¹⁶ magnetron sputtering¹⁷ and hot-pressing.¹⁸ However, problems remain for most of these methods such as high-energy consumption and the need for expensive and sophisticated instruments. Additionally, expensive poisonous agents (fluorinated components) were used to achieve superhydrophobic surfaces in many studies.^{19–21} Compared to fluorosilanes, PDMS not only has low surface energy but is also less toxic, cheaper, thermally stable and durable than many polymers, suggesting that PDMS may serve as both a structural precursor and a raw modifying material.^{22,23} Due to its low intrinsic surface energy and moldability, many kinds of nanomaterials and polymers such as ZnO,²⁴ carbon nanowalls²⁵ and epoxy resin²⁶ were doped with PDMS. Due to suitable preparation process, controllable particle size and good reactivity with

organic groups, SiO₂ nanoparticles are the most widely applied materials in superhydrophobic surfaces.^{27,28} Because the aggregation of nanoparticles results in multi-scale roughness and PDMS provides good hydrophobicity with non-polar –CH₃ groups, the composites containing SiO₂ nanoparticles and PDMS have attracted much attention in recent decades. Few papers investigating the thermal and mechanical stabilities of durable superhydrophobic coatings on glass have been reported, which constraints wide applications of superhydrophobic coating.

Herein, silica aerogel/PDMS composites were synthesized using a typical sol-gel method and subsequent PDMS chemical modification. Interface adhesive (Qsil 216) was used to enhance the adhesion between the superhydrophobic coating and the glass substrate. The preparation was simple and scalable by spraying Qsil 216 and silica aerogel/PDMS composites in order. The semi-transparent superhydrophobic coating was found to be self-cleaning and durable with excellent thermal and mechanical stabilities.

2. Results and discussion

2.1 Surface morphology and chemical composition

Fig. 1 shows a schematic illustration of the superhydrophobic coating. MSA possessed great quantities of non-polar groups (–CH₃), but it was difficult to form pure MSA coating on the glass base due to the weak cross-linking interaction. It has been recognized that PDMS with high viscosity and low surface energy has good connectivity for its end hydroxyl groups and long polymer chains, which are flexible and rotatable. Thus, P-

^aMIIT Key Laboratory of Critical Materials Technology for New Energy Conversion and Storage, School of Chemistry and Chemical Engineering, Harbin Institute of Technology, Harbin, 150001, PR China. E-mail: hit_liji@163.com

^bDepartment of Chemistry, Rice University, Houston, Texas 77005, USA



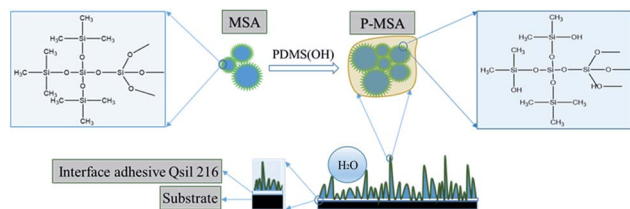


Fig. 1 Schematic of the chemical composition of MSA and P-MSA and the micromorphology of the superhydrophobic coating.

MSA exhibited stable and controllable morphology and overcame the fragile features of MSA.

Fig. 2 shows the presence of rough micromorphology. Comparing Fig. 2(a), (d) and (g) with Fig. 2(b), (e) and (h), respectively, it was found that the aerogel particles modified by PDMS stacked more intensely and irregularly, implying that the coatings possessed better film-formation properties than before. As seen in Fig. 3(a), (d), and (g), whether or not TMCS or HTMS was added, the particles aggregated more seriously and even became indistinguishable due to the presence of a silane coupling agent. As shown in Fig. 2(b), (e) and (h), the P-MSA-II sample exhibited the most serious aggregation and the smallest porosity. It was speculated that the residual hydroxyl groups on the surface of MSA-II were more than those on MSA-I and MSA-III because of the vigorous hydrolysis of TMCS.

As we know, the hierarchical micro/nanoscale structure on the surface is essential for superhydrophobic coatings besides chemical composition with low surface energy.²⁹ This was achieved by pores, clusters of silica aerogel bulks and silica aerogel particles, which are marked in Fig. 2(b), (d) and (e), respectively. The globular entities and pores were less than 300 nm in diameter, whereas the sizes of the clusters of silica aerogel bulk were approximately more than 1 μm in the micron level. Notably, globular entities were coarse and composed of small mastoid nanoparticles. The three-dimensional micromorphologies of P-MSA-I, P-MSA-II and P-MSA-III coatings obtained using AFM are shown in Fig. 2(c), (f) and (i), respectively, and these results confirmed the existence of a hierarchical micro/nanoscale structure, corresponding to previous analysis results based on SEM images.

FTIR spectra showed the functional groups of different aerogels before and after PDMS modification (Fig. 3). The peak at

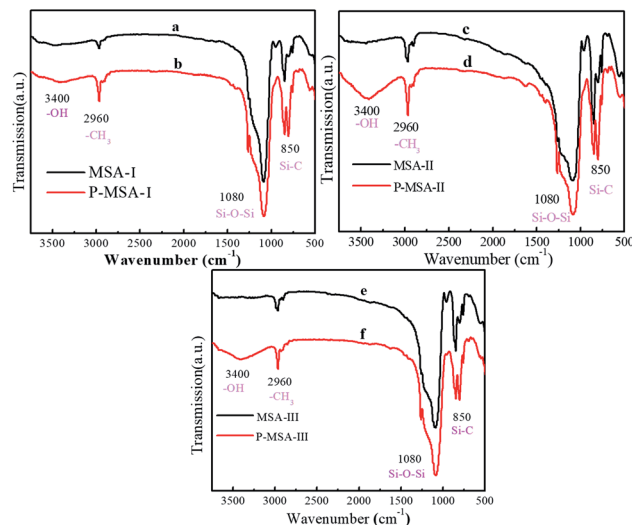


Fig. 3 FTIR spectra of (a) MSA-I, (b) P-MSA-I, (c) MSA-II, (d) P-MSA-II, (e) MSA-III, and (f) P-MSA-III coatings.

2960 cm^{-1} was related to the $-\text{CH}_3$ groups, and the broad band centered at 3400 cm^{-1} was ascribed to O–H stretching in the Si–OH groups. The bands located at 1103, 953, and 801 cm^{-1} were associated with the Si–O–Si asymmetric bond stretching vibration, the Si–OH stretching vibration, and the network Si–O–Si symmetric bond stretching vibration, respectively.^{16,30} It was clearly observed that many hydroxyl groups remained in three nanocomposites due to the modification of PDMS. Additionally, the intensity of the peaks corresponding to the methyl group increased. PDMS, which was loaded with many methyl groups, provided good hydrophobic properties. Most importantly, PDMS provided many abundant hydroxyl groups due to which the coatings possessed good adhesion with substrates such as glass and paper.

2.2 Static and dynamic wetting properties of three coatings

As shown in the lower-left corner of Fig. 2(b), (e), and (h), it is clear that the water droplets adopted a perfect ball shape, which implied excellent superhydrophobicities of the corresponding coatings. Furthermore, the hydrophobicities of the three P-MSA coatings are quantitatively shown in Table 1 including advancing angle, receding angle and contact angle. The water contact angles of the three samples were higher than 150°. The results were consistent with the droplet shapes in Fig. 2(b), (e), and (h). It was speculated that the superhydrophobic property resulted from the synergistic effect of MSAs and PDMS. On the one hand, nanoparticles tended to agglomerate due to high surface area and surface energy. The inter-particle forces within

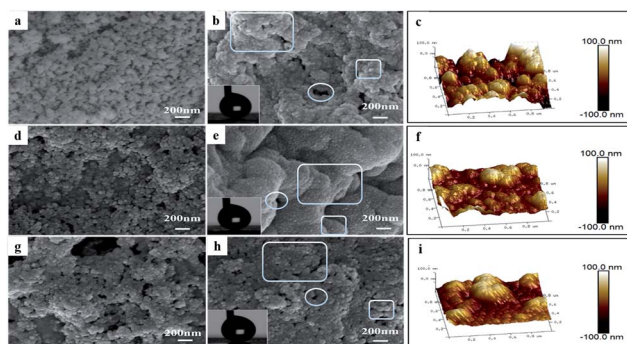


Fig. 2 SEM and AFM images of (a) MSA-I, (b) and (c) P-MSA-I, (d) MSA-II, (e) and (f) P-MSA-II, (g) MSA-III, and (h) and (i) P-MSA-III coatings.

Table 1 WCA and sliding angle of P-MSA coatings

Coatings	θ_{CA}	θ_{Adv}	θ_{Rec}
P-MSA-I	160.81 \pm 4°	169.80 \pm 3°	166.18 \pm 3°
P-MSA-II	163.28 \pm 5°	165.80 \pm 3°	155.96 \pm 3°
P-MSA-III	165.75 \pm 3°	169.36 \pm 3°	162.37 \pm 3°



Table 2 The naming, precursor and methylation agent of methylated silica aerogels (MSAs)

Silica aerogels	Precursor	Methylation agent
MSA-I	Sodium silicate	TMCS
MSA-II	TEOS	TMCS
MAS-III	TEOS	HMDS

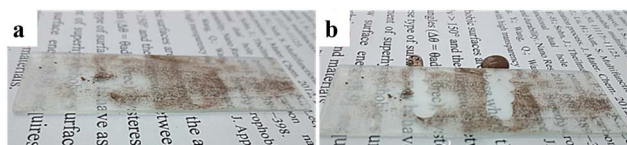
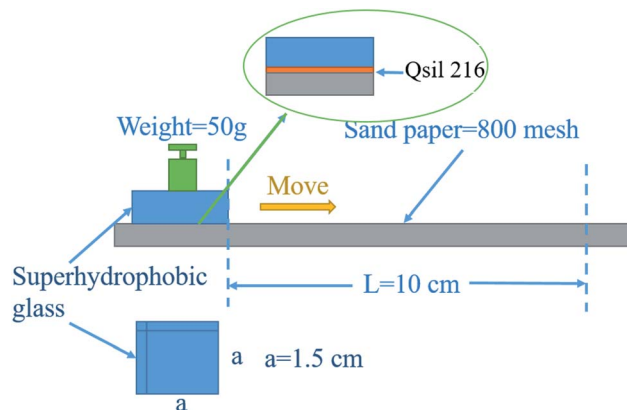
the agglomerates originated from van der Waals, capillary, and electrostatic forces.³¹ MSAs, made up of aggregated nanoparticles, provided a multi-scale hierarchical structure with granular bulges and pores, which could trap sufficient air pockets on the rough interstices between liquid and solid.¹⁶ Therefore, the water drop could remain on the layer of air with minimum solid fraction in contact. On the other hand, the guest phase (MSAs) was uniformly and completely coated by the host matrix (PDMS) (Fig. 2), which gave rise to the enhancement of hydrophobic methyl groups (Fig. 3). The contact angle hysteresis ($\theta_{CAH} = \theta_{Adv} - \theta_{Rec}$) was less than 10° among the three samples and thus, the droplets could easily slide away from the coating. This resulted in the non-continuous solid/liquid/gas three-phase contact line. The spherical droplets on the surface of the superhydrophobic coatings showed Cassie–Baxter's state with almost no sticking towards the surface.³² Furthermore, these superhydrophobic coatings were intact under normal circumstances for a period of more than 6 months.

2.3 Self-cleaning properties

Alternative surfaces that clean themselves by water flow are known as self-cleaning surfaces. Especially on superhydrophobic surfaces, the accumulated dust particles can be easily washed off by rolling water drops.^{33,34} The self-cleaning property of the superhydrophobic P-MSA-I coating was verified, as shown in Fig. 4. The P-MSA-I coating was contaminated at first by dust particles, as shown in Fig. 4(a). A hanging droplet of nearly $15 \mu\text{l}$ was produced from a syringe and slowly dragged on the dust-accumulated area. The droplets effectively collected the dust particles while rolling on the surface rapidly due to the extremely low sliding angle.

2.4 Abrasion resistance stability

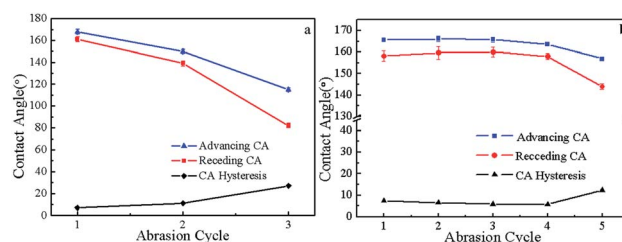
Objective comparison of the abrasion resistance of superhydrophobic surfaces has been hampered by the lack of a single, standardized test method.³⁵ There are many methods to analyse the mechanical properties of superhydrophobic coatings including the pencil hardness test, the sandpaper test, the scotch tape test, and the water drop/jet impact test.^{36–38} The

**Fig. 4** Optical images of (a) the heavily dusty surface and (b) the self-cleaned surface of the superhydrophobic P-MSA-I coating.**Fig. 5** Schematic of the abrasion test employed to evaluate the robustness on the superhydrophobic coating.

methodology illustrated in Fig. 5 was applied. Sand paper (800 mesh) served as an abrasive surface, and the P-MSA-I coating was tested facing this abrasive material. While a pressure ($\sim 2178 \text{ Pa}$) was applied vertically to the glass, the glass slide was moved in one horizontal direction. The advancing contact angle, receding contact angle and hysteresis changes of the coating were then measured after abrasion (10 cm in abrasion length), as shown in Fig. 6.

The pure P-MSA-I coating showed poor mechanical stability, and the superhydrophobic surface was damaged completely after two abrasion cycles. However, the P-MSA-I/Qsil 216 surface remained superhydrophobic after going through at least four abrasion cycles. Even so, the contact angle hysteresis was less than 10° , which indicated that a small loading of Qsil 216 on the glass has better durability against mechanical force. PDMS, a soft polymer, could be easily scratched away from the surface. Thus, the optimum material should be obtained between the inorganic phase basement and the polymer to achieve improved mechanical stability of the coating, which in our case was the coating prepared by the addition of Qsil 216 on the surface of the basement.

It is well-known that glass is a dense silicate material with extremely poor conductivity; the chemical composition and surface texture are different from those of metal and fabric. As a result, many polymers cannot be integrated with glass substrates by electrostatic interaction or molecular diffusion. Due to the presence of many activated functional groups, such as $-\text{Si}-\text{OH}$ groups, in the curing process, firm adhesion can

**Fig. 6** The effect of the sand paper abrasion cycle on the advancing contact angle, receding contact angle and contact angle hysteresis in (a) the absence of Qsil 216 and (b) the presence of Qsil 216.

occur because of strong intermolecular forces and chemical bonds between the adhesive and glass. Additionally, P-MSAs can adhere well on the surface of Qsil 216, indicating that the adhesive has lower surface tension than PDMS, which is more propitious to wetting the surface of glass.

2.5 Optical transparency

As shown in Fig. 7, pure glass transmission was about 85% in the visible range from 350 to 770 nm. When P-MSA-I was coated on the glass, the transmission decreased to 72%. Even when the P-MSA-I/Qsil 216 composite was coated, the transmission decreased to 60%, which was 70.95% of the pure glass transmission. The semi-transparent superhydrophobic glass met most of the requirements for practical applications.

2.6 Thermal stability

The thermal stability was tested at the gradient of 50 °C from 150 °C to 400 °C, and the tests were carried out at a rate of 10 °C min⁻¹ under air atmosphere for 4 h under ultimate temperature. From Fig. 8, it can be observed that the coating maintained superhydrophobic features up to 350 °C. At 400 °C, the local area of the P-MSA-I coating became hydrophilic. It was speculated that the continuous high-temperature conditions resulted in the loss of weight and therefore caused irreversible damage to the microstructure. The effects of temperature on the advancing contact angle, the receding contact angle and the contact angle hysteresis are shown in Fig. 9. The coating possessed excellent superhydrophobic features (θ_{Adv} , $\theta_{Rec} \geq 155^\circ$) and remarkable self-cleaning properties ($\theta_{CAH} \leq 10$) (Fig. 9).

3. Experimental

3.1 Materials

The compounds used were hydroxyl-terminated polydimethylsiloxane (PDMS, AR, $M = 1000$, Guangzhou Juchengzhaoye Organosilicon Material Co. China),

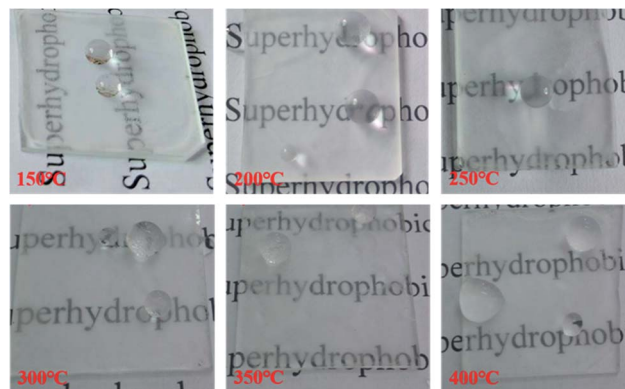


Fig. 8 Optical images of water droplets on the glass coated by the P-MSA-I/Qsil 216 composite after high temperature calcination for 4 h.

tetraethylorthosilicate (TEOS, AR, Tianjin Kermel Chemical Reagents Co. China), and Qsil 216 (ACC-SILICONS). Other reagents were supplied by Xilong Chemical Co., China and used as received including dimethylfumarate (DMF, AR), toluene (AR), isopropyl alcohol (AR), acetone (AR), sodium silicate (AR), trimethylchlorosilane (TMCS, AR), hexane (AR), hexamethyldisilazane (HMDS, AR), $\text{NH}_3 \cdot \text{H}_2\text{O}$ (1 mol ml⁻¹) and hydrochloric acid (HCl, 1 mol ml⁻¹).

3.2 Preparation of methylated silica aerogel (MSA)

Ten g TEOS was hydrolysed and polymerized in a solution of 22.08 g ethanol, 2.59 g water and 0.3 ml HCl for 4 h at 85 °C. Then, 9.8 ml $\text{NH}_3 \cdot \text{H}_2\text{O}$ and 1.58 g DMF were dripped into the above-mentioned solution and gelled for 8 h at 35 °C. The gel was aged further to strengthen the gel network and resist collapse during ambient drying by a two-pot method. A 50 ml EtOH/H₂O solution (4v% : 1v%) was added into the above-mentioned solution and kept for 12 h and then, the 50 ml EtOH/TEOS solution (4v% : 1v%) was added and kept for 24 h. The as-prepared silicon aerogel was named as SA.

To obtain methylated silicon aerogel, methylation agents including TMCS/hexane (15v% : 85v%) or HMDS/hexane

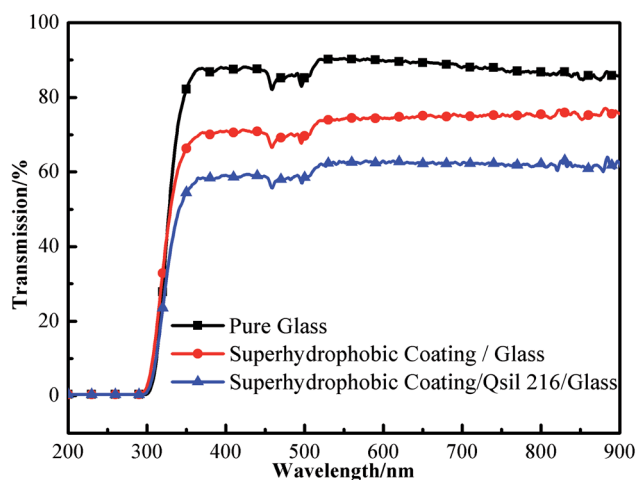


Fig. 7 Optical transmission spectra of pure glass, the glass coated by P-MSA-I and the glass coated by P-MSA-I/Qsil 216 composite.

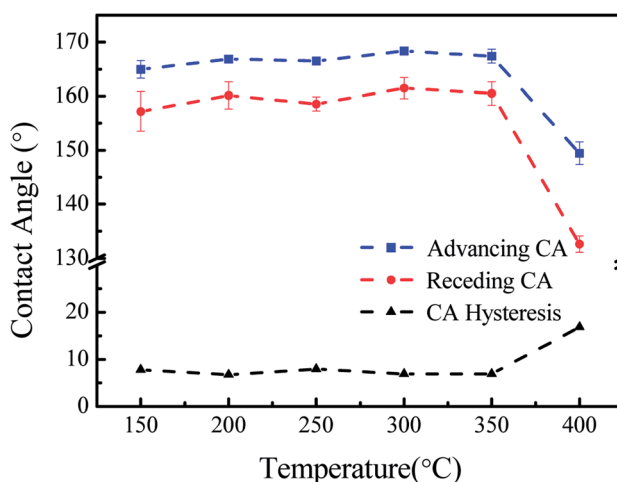


Fig. 9 The effects of temperature on the advancing contact angle, the receding contact angle and the contact angle hysteresis.



(15_{v%} : 85_{v%}) solutions were added in SA with strong stirring for 12 h. Subsequently, solvents were rinsed by 50 ml ethanol and hexane (4_{v%} : 1_{v%}) 4 times at 50 °C and then thoroughly dried from 60 to 160 °C at a rate of 20 °C every 4 h; the obtained aerogels were named as “MSA-II” and “MAS-III”.

Additionally, for the MSA-I sample, silicon sol was obtained by the ion exchange method using sodium silicate as the silicon source, and the subsequent procedures were similar to those of the others.

3.3 Preparation of methylated silica Aerogel/PDMS composite (P-MSA)

MSA samples were smashed by ball mill grinding for 10 min at room temperature. One g MSA was modified by 0.6 g PDMS in 100 ml of toluene with stirring for 48 h. P-MSA was centrifuged with acetone and dried at 100 °C for 6 h (Table 2).

3.4 Composite coatings

The solutions of Qsil 216 silicon part-A (1 g) and hexane (50 ml) were stirred completely. Then, 0.1 g Qsil 216 silicon part-B was added. The solution was sprayed on the substrate and dried at 80 °C for 30 min. The P-MSA suspension, which was prepared by isopropyl alcohol with a concentration of 10 mg ml⁻¹, was sprayed onto the Qsil 216 layer and then, the coating was dried at 80 °C for 2 h.

3.5 Characterization of the P-MSA coatings

The water contact and sliding angles were measured by an instrument (JC2000C, China) at room temperature. The roughness and morphology of the coating surface were characterized by atomic force microscopy (AFM, Dimension Icon, Germany) and scanning electron microscopy (SEM, SUPRA 55, Germany). The components of the materials were analysed by Fourier transform infrared spectroscopy (FTIR, Bruker TENSOR27, Germany).

4. Conclusions

A facile and scalable method to prepare superhydrophobic coatings was reported in detail. The semi-transparent coatings exhibited excellent durability, self-cleaning, and superhydrophobicity as well as excellent thermal and mechanical stabilities. The advancing water contact angle and sliding angle were 169.80 ± 3° and 4°, respectively, and these were remarkable results. The coating maintained water repellency under 350 °C for at least 4 h and possessed durable superhydrophobicity for 6 months at ambient conditions. Additionally, it remained superhydrophobic after at least four rounds of abrasion with sandpaper under more than 2000 Pa. This novel coating with self-cleaning, antifouling, low-drag, and anti-smudge properties can be used in applications where superhydrophobicity is important.

Conflicts of interest

There are no conflicts to declare.

Acknowledgements

This work is supported by the Daqing Oilfield Postdoctorate Working Station. The authors also appreciate the financial support of “the Fundamental Research Funds for the Central Universities” (Grant No. HIT. NSRIF. 2017026), the Program of Heilongjiang Province (Project No. GC13A105), the National Natural Science Foundation of China (Grant No. 51302052), and the National Science Fund for Distinguished Young Scholars of China (Grant No. 51325201).

Notes and references

- 1 T. M. Schutzius, I. S. Bayer, M. K. Tiwari and C. M. Megaridis, *Ind. Eng. Chem. Res.*, 2011, **50**, 11117–11123.
- 2 L. Feng, Z. Yan, X. Qiang, Y. Liu and Y. Wang, *Appl. Phys. A*, 2016, **122**, 165.
- 3 X. Du, J. S. Li, L. X. Li and P. A. Levkin, *J. Mater. Chem. A*, 2012, **1**, 1026–1029.
- 4 X. Du, X. Li and J. He, *ACS Appl. Mater. Interfaces*, 2010, **2**, 2365–2372.
- 5 M. Fang, Z. Tang, H. Lu and S. Nutt, *J. Mater. Chem.*, 2011, **22**, 109–114.
- 6 H. Jin, M. Kettunen, A. Laiho, H. Pynnönen, J. Paltakari, A. Marmur, O. Ikkala and R. H. Ras, *Langmuir*, 2011, **27**, 1930–1934.
- 7 W. Zhang, Z. Shi, F. Zhang, X. Liu, J. Jin and L. Jiang, *Adv. Mater.*, 2013, **25**, 2071–2076.
- 8 S. Hoshian, V. Jokinen, V. Somerkivi, A. R. Lokanathan and S. Franssila, *ACS Appl. Mater. Interfaces*, 2015, **7**, 941.
- 9 J. Cheng, Y. Zhang, Q. Wang and T. Wang, *J. Appl. Polym. Sci.*, 2013, **129**, 2959–2965.
- 10 P. Wang, H. Han, J. Li, X. Fan, H. Ding and J. Wang, *Appl. Phys. A*, 2016, **122**, 53.
- 11 H. Ogihara, J. Xie, J. Okagaki and T. Saji, *Langmuir*, 2012, **28**, 4605–4608.
- 12 G. R. J. Artus and S. Seeger, *Ind. Eng. Chem. Res.*, 2012, **51**, 2631–2636.
- 13 S. H. Park, S. M. Lee, H. S. Lim, J. T. Han, D. R. Lee, H. S. Shin, Y. Jeong, J. Kim and J. H. Cho, *ACS Appl. Mater. Interfaces*, 2010, **2**, 658.
- 14 K. C. Chang, H. I. Lu, C. W. Peng, M. C. Lai, S. C. Hsu, M. H. Hsu, Y. K. Tsai, C. H. Chang, W. I. Hung and Y. Wei, *ACS Appl. Mater. Interfaces*, 2013, **5**, 1460–1467.
- 15 D. Ebert and B. Bhushan, *Langmuir*, 2012, **28**, 11391.
- 16 X. Du and J. He, *ACS Appl. Mater. Interfaces*, 2011, **3**, 1269–1276.
- 17 M. Petr, J. Hanuš, O. Kylián, J. Kratochvíl, P. Solař, D. Slavinská and H. Biederman, *Mater. Lett.*, 2016, **167**, 30–33.
- 18 S. Gao, J. Huang, S. Li, H. Liu, F. Li, Y. Li, G. Chen and Y. Lai, *Mater. Des.*, 2017, **128**, 1–8.
- 19 K. Ellinas, S. P. Pujari, D. A. Dragatogiannis, C. A. Charitidis, A. Tserepi, H. Zuilhof and E. Gogolides, *ACS Appl. Mater. Interfaces*, 2014, **6**, 6510.
- 20 S. M. Kang, S. M. Kim, H. N. Kim, M. K. Kwak, D. H. Tahk and K. Y. Suh, *Soft Matter*, 2012, **8**, 8563–8568.



- 21 Z. Pan, H. Shahsavan, W. Zhang, F. K. Yang and B. Zhao, *Appl. Surf. Sci.*, 2015, **324**, 612–620.
- 22 X. Liu, Y. Xu, K. Ben, Z. Chen, Y. Wang and Z. Guan, *Appl. Surf. Sci.*, 2015, **339**, 94–101.
- 23 X. Liu, Y. Wang, Z. Chen, K. Ben and Z. Guan, *Appl. Surf. Sci.*, 2016, **360**, 789–797.
- 24 G. Ren, Y. Song, X. Li, B. Wang, Y. Zhou, Y. Wang, B. Ge and X. Zhu, *J. Colloid Interface Sci.*, 2018, 57–62.
- 25 L. Zhang, C. H. Xue, M. Cao, M. M. Zhang, M. Li and J. Z. Ma, *Chem. Eng. J.*, 2017, **320**, 244–252.
- 26 Y. Zhang, F. Ren and Y. Liu, *Appl. Surf. Sci.*, 2018, **436**, 405–410.
- 27 W. Ding, Z. Zhang, Y. Li and C. Xu, *ACS Appl. Mater. Interfaces*, 2014, **5**, 10014–10021.
- 28 L. Xu, R. G. Karunakaran, J. Guo and S. Yang, *ACS Appl. Mater. Interfaces*, 2012, **4**, 1118.
- 29 A. Lafuma and D. Quéré, *Nat. Mater.*, 2003, **2**, 457–460.
- 30 Q. F. Xu, J. N. Wang and K. D. Sanderson, *ACS Nano*, 2010, **4**, 2201–2209.
- 31 Y. Raichman, M. Kazakevich, E. Rabkin and Y. Tsur, *Adv. Mater.*, 2006, **18**, 2028–2030.
- 32 S. Liu, S. S. Latthe, H. Yang, B. Liu and R. Xing, *Ceram. Int.*, 2015, **41**, 11719–11725.
- 33 S. Pitchaimuthu, S. S. Latthe, C. Ravidhas, C. A. Jennifer, K. D. David, R. Venkatesh, A. Devadoss, C. Terashima, K. Nakata and A. Fujishima, *Crystengcomm*, 2015, **17**, 2624–2628.
- 34 Y. Lu, S. Sathasivam, J. Song, C. R. Crick, C. J. Carmalt and I. P. Parkin, *Science*, 2015, **347**, 1132–1135.
- 35 T. Verho, C. Bower, P. Andrew, S. Franssila, O. Ikkala and R. H. Ras, *Adv. Mater.*, 2011, **23**, 673–678.
- 36 Y. Xiu, Y. Liu, D. W. Hess and C. P. Wong, *Nanotechnology*, 2010, **21**, 155705.
- 37 S. Liu, X. Liu, S. S. Latthe, G. Li, S. An, S. S. Yoon, B. Liu and R. Xing, *Appl. Surf. Sci.*, 2015, **351**, 897–903.
- 38 S. S. Latthe, C. Terashima, K. Nakata, M. Sakai and A. Fujishima, *J. Mater. Chem. A*, 2014, **2**, 5548–5553.

